Fast sizing of the width of infinite vertical cracks using Constant Velocity Flying-Spot thermography

J. González[1,2], A. Mendioroz[1], A. Sommier[3], J.C. Batsale[3], C. Pradere[3] and A. Salazar[1,*]

[1]Departamento de Física Aplicada I, Escuela de Ingeniería de Bilbao, Universidad del País Vasco UPV/EHU, Plaza Ingeniero Torres Quevedo 1, 48013 Bilbao, Spain.

[2]Department of Applied Physics, CINVESTAV Unidad Mérida, carretera Antigua a Progreso km 6, A.P. 73 Cordemex, Mérida Yucatán 97310, Mexico.

[3]I2M-TREFLE, UMR CNRS 5295, Esplanade des Arts et Métiers 33405 Talence Cedex, France.

*Corresponding author, E-mail address: agustin.salazar@ehu.es

Abstract

Constant Velocity Flying-Spot thermography consists in scanning the sample surface by a focused CW-laser spot moving at constant speed. This technique was designed to study large surfaces in short times. In this work, we propose a method, based on a Flying-Spot thermography setup, to size the width of vertical cracks by fitting the temperature profile along the line that contains the center of the laser spot and is perpendicular to the crack to its analytical expression. This method is also valid in the opposite configuration, where the laser spot remains at rest and the sample is moving at constant velocity. This configuration is useful for in-line inspection in factories, for detecting and sizing cracks in real time, without stopping the production chain. Experimental measurements on stainless steel samples containing calibrated vertical cracks confirm the validity of the method to measure the crack width with high accuracy, even for submicronic wide cracks.

Keywords: infrared thermography, flying-spot thermography, nondestructive evaluation, cracks detection.

1. Introduction

The growing necessity of in-service non-destructive testing and evaluation of surface breaking cracks in a wide variety of devices has been a challenging task for modern industries and laboratories. Several non-destructive techniques, like dye penetrants, magnetic particles, eddy currents and X-rays have been widely used to detect fissures. In the last decades, optically stimulated infrared (IR) thermography has gained attention because it is noncontact, safe and very sensitive to the presence of cracks [1-4]. To detect this kind of defects, a focused laser beam is directed to the sample surface close to the crack, which produces an asymmetry in the heat flux. In the case of infinite vertical cracks, an analytical solution of the surface temperature can be found for both lock-in and pulsed excitation. By fitting the surface temperature recorded by an IR camera to the analytical model the width of the crack was obtained [5,6]. For finite vertical cracks, the surface temperature has to be obtained numerically, and the depth and width of the crack can be obtained by analyzing the infrared thermogram [7-9].

In the nineties of the last century, following pioneering works performed two decades before [10-11], it was introduced the so-called Flying-Spot thermography to study large surfaces in short times [12]. It consists in illuminating the sample surface with a moving laser spot or line and detecting the time evolution of the surface temperature with an infrared camera [12-20]. The sample can be heated by a continuous wave [12-16], modulated [18] or pulsed laser [17-20]. This technique allows detecting cracks a few micrometers wide [17]. Recently, several approaches to characterize the geometrical parameters of the crack (depth, length, width, orientation…) have been introduced by several research groups [21-27]. They take advantage of the asymmetry of the temperature field at both sides of the crack arising from the thermal resistance produced by the crack, which partially blocks heat flux when the laser spot approaches the crack. Moreover, Flying-Spot thermography has been recently proposed to map the thermal diffusivity in heterogeneous and (an)isotropic samples [28-30].

The aim of this work is to size the width of vertical cracks accurately using a Flying-Spot thermography setup. First, we find an analytical expression for the surface temperature of a sample containing a vertical crack when the surface is scanned by a focused CW-laser spot moving at constant speed. The signature of the crack is a temperature discontinuity at the crack position. We analyze the dependence of this temperature jump on the experimental parameters: laser speed, laser radius, crack width and sample thermal properties. We propose a method to size the width of vertical cracks by fitting the temperature profile along the line that contains the center of the laser spot and is perpendicular to the crack to the analytical model. Note that

this method can be directly applied when the laser spot remains at rest and the sample is moving at constant velocity, just by performing a Galilean transformation of coordinates. This is of special interest for in-line production or in-line quality control processes in factories, where cracks must be detected in real time, without stopping the production chain. Experimental measurements on stainless steel samples containing calibrated vertical cracks indicate that the method is very sensitive to detect submicronic cracks. Moreover, by fitting the temperature profiles to the analytical model, the width of the crack is obtained with high accuracy.

2. Theory

Figure 1 represents a semi-infinite and opaque material containing an infinite vertical crack placed at plane $y = 0$. The sample is illuminated by a Dirac-like laser pulse of energy Q_o and Gaussian profile of radius a (at $1/e^2$ of the intensity). The center of the laser spot is located at a distance d from the crack. Adiabatic boundary conditions at the sample surface have been assumed. The temperature profile along the y-axis is given by (see Eq. (10) in Ref. [6]):

$$T(0,y,0,t) = \frac{2Q_o\eta}{\varepsilon\sqrt{\pi^3 t}} \frac{e^{-\frac{2(y-d)^2}{a^2+2\mu^2}}}{a^2+2\mu^2} + \tag{1}$$

$$+\operatorname{sign}(y) \frac{Q_o}{\varepsilon\pi^2 a\sqrt{t}\mu\sqrt{a^2+2\mu^2}} \int_{-\infty}^{\infty} \mathrm{d}y_o \operatorname{sign}(y_o) e^{-\frac{2(y_o-d)^2}{a^2}-\frac{u^2}{\mu^2}} \left[1 - \frac{\sqrt{\pi}\mu}{KR_{th}} e^{\left(\frac{\mu}{KR_{th}}+\frac{u}{\mu}\right)^2} \operatorname{erfc}\left(\frac{\mu}{KR_{th}}+\frac{u}{\mu}\right) \right],$$

where η is the energy fraction absorbed by the sample, $\mu = \sqrt{4Dt}$ is the thermal diffusion length (m), erfc is the complementary error function, K, D and ε are the thermal conductivity ($Wm^{-1}K^{-1}$), thermal diffusivity (m^2s^{-1}) and thermal effusivity ($Js^{-0.5}m^{-2}K^{-1}$) respectively. $u = |y| + |y_o|$, where y_o indicates the y coordinates covered by the laser spot; integration is performed to add the contribution of the whole Gaussian profile. R_{th} is the thermal contact resistance ($W^{-1}m^2K$) of the crack, which is related to the crack width (m), L, through the equation $R_{th} = L/K_{air}$ [31].

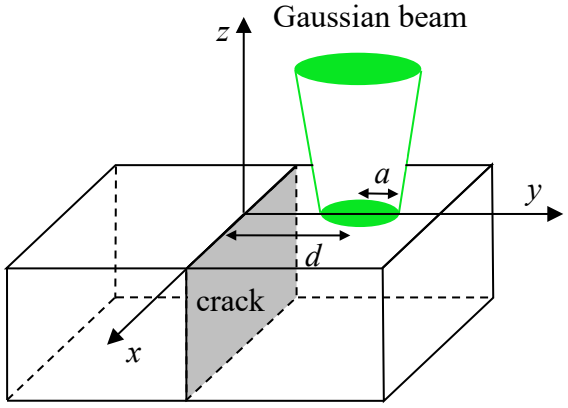

Figure 1. Scheme of a semi-infinite sample which contains an infinite vertical crack (in grey) and that is illuminated by a brief laser pulse of Gaussian profile.

Now we consider that a CW-laser of power P_o and Gaussian profile of radius a (at $1/e^2$) moving along the y-axis to the right at constant velocity v, while the material remains at rest, as it is shown in Fig. 2a. The laser was switched on at $t = -t_o$. The temperature profile along the y-axis at time t is given by the convolution integral of Eq. (1):

$$T(0,y,0,t)=\frac{2P_o\eta}{\varepsilon\sqrt{\pi^3}}\int_{-t_o}^{t}\frac{1}{\sqrt{t-\tau}}\frac{e^{-\frac{2(y-v\tau)^2}{a^2+8D(t-\tau)}}}{a^2+8D(t-\tau)}d\tau+$$

$$+\operatorname{sign}(y)\frac{P_o}{\varepsilon\pi^2 a\sqrt{D}}\int_{-\infty}^{\infty}dy_o\int_{-t_o}^{t}d\tau\frac{\operatorname{sign}(y_o)}{t-\tau}\frac{e^{-\frac{2(y_o-v\tau)^2}{a^2}-\frac{u^2}{4D(t-\tau)}}}{\sqrt{a^2+8D(t-\tau)}}\times \tag{2}$$

$$\times\left[1-\frac{\sqrt{4\pi D(t-\tau)}}{KR_{th}}\exp\left(\left(\frac{\sqrt{4\pi D(t-\tau)}}{KR_{th}}-\frac{u}{\sqrt{4\pi D(t-\tau)}}\right)^2\right)\right]\operatorname{erfc}\left(\frac{\sqrt{4D(t-\tau)}}{KR_{th}}+\frac{u}{\sqrt{4D(t-\tau)}}\right).$$

Here sign(x) is: -1 when $x < 0$, +1 when $x > 0$ and 0 when $x = 0$. In the previous expression the origin of time is taken in such a way that at time $t = 0$ the laser is at the origin of the reference frame.

According to the relativity principle, by performing a Galilean transformation in Eq. (2), we calculate the temperature profile when the laser remains at rest while the material is moving at constant velocity along the y-axis to the left (see Fig. 2b). This means that exponents $(y_o\text{-}v\tau)^2$ and $(y\text{-}v\tau)^2$ must be replaced by $(y_o\text{+}vt\text{-}v\tau)^2$ and $(y\text{+}vt\text{-}v\tau)^2$ respectively.

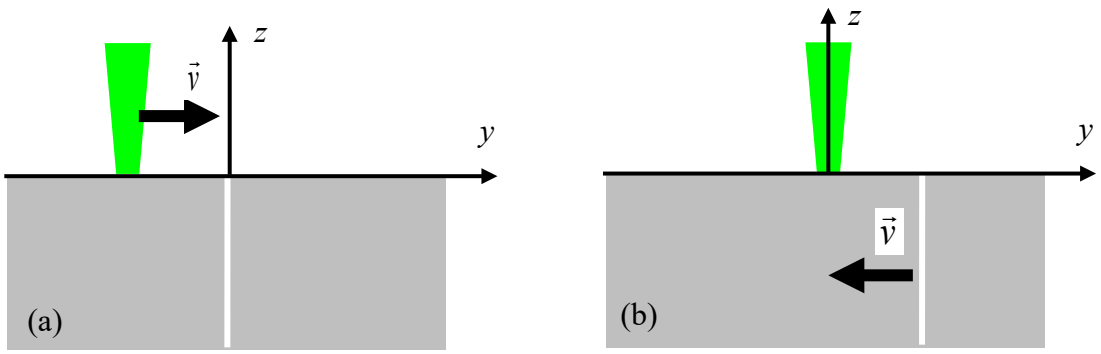

Figure 2. Cross section of the cracked sample. (a) The laser is moving to the right at constant speed v. (b) The laser is fixed and the sample is moving to the left at constant speed v.

3. Simulations

In this section, we show numerical calculations of the temperature profile along the y-axis of a cracked sample, using Eq. (2), to analyze the effect of the different parameters in the visibility of the crack: the thermal resistance (R_{th}), the laser radius (a) and the distance between laser and crack ($d = vt$). Simulations are performed for an AISI-304 stainless steel sample (D = 4.0 mm^2s^{-1} and K = 15 $Wm^{-1}K^{-1}$).

Figure 3 shows a sequence of temperature profiles along the y-axis for an AISI-304 sample with an infinite vertical crack located at $y = 0$. The laser spot is moving from left to right at constant speed v = 10 mm/s. The power of the laser is P_o = 1 W and its radius is a = 0.3 mm. Five position of the laser spot are shown: y = -1, -0.5, 0, 0.5 and 1 mm. For each position, three crack widths are considered: L = 25, 2.5 and 0.25 μm. As can be observed, the signature of the crack is an abrupt temperature discontinuity, which increases with the crack width. Note that even submicronic cracks can be detected. In this way, it is worth mentioning that, according to Eq. (2), the thermal resistance is correlated to the thermal conductivity of the material through the factor KR_{th}. This means that narrow cracks are better detected in good thermal conducting materials (metals, alloys, ceramics, etc.) than in thermal insulators (polymers, composites, etc.).

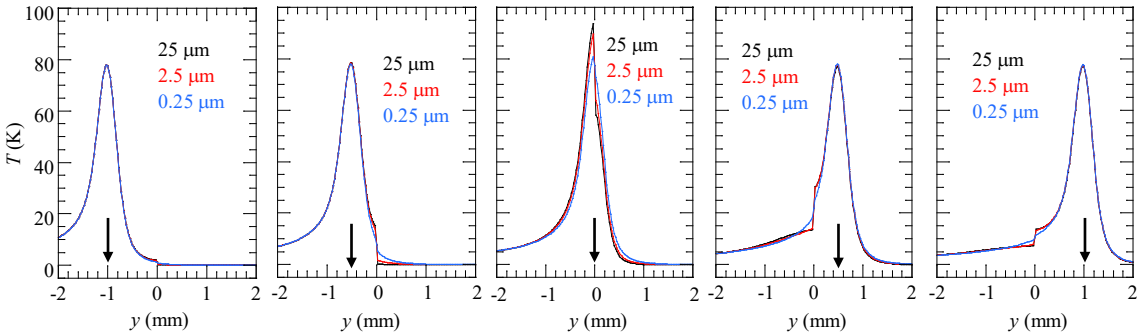

Figure 3. Sequence of temperature profiles for an AISI-304 sample with an infinite vertical crack located at y = 0. The laser spot is moving from left to right at constant speed v = 10 mm/s. The power of the laser is P_o = 1 W and its radius is a = 0.3 mm. Each figure corresponds to a different position of the laser spot, which is marked by the arrow: y = -1, -0.5, 0, 0.5, 1 mm. In each figure, three crack widths are analyzed.

In order to quantify the dependence of the temperature jump at the crack position on the experimental parameters, we define the normalized temperature contrast at the crack as

$$\Delta(t) = \frac{T(0,0^-,0,t) - T(0,0^+,0,t)}{T(0,d=vt,0,t)}, \tag{3}$$

which is independent of the laser power P_o.

Figure 4a shows the temperature contrast as a function of the crack width in an AISI-304 sample. This simulation is performed for a laser spot of radius a = 0.4 mm, moving at v = 10 mm/s, when the laser spot is just arriving at the crack position, i.e. d = -a, as shown in the inset of Fig. 4a. As can be observed, Δ has a sigmoidal shape where three regions of interest can be distinguished. For narrow cracks, $L \leq 0.03$ μm, the temperature contrast is so small that they remain undetected. For wide cracks, $L \geq 20$ μm, the temperature contrast is very high and therefore they can detected easily, but they cannot be sized since there is no sensitivity, i.e. different widths produce the same temperature contrast. Finally, for intermediate widths, 0.1 μm $\leq L \leq$ 10 μm, fissures can be detected and sized. This is the region we are interested in this work.

In Fig. 4b we analyze the influence of the laser spot radius on the temperature contrast. Simulations are performed for AISI-304 and the laser spot moving at v = 10 mm/s and d = - 0.4 mm. As can be observed, Δ increases with a, even when the laser spot overlaps the crack. However, for a practical point of view, it is better to avoid the laser spot overlapping the fissure to prevent the light from entering inside the crack and disturbing the temperature profile. Accordingly, in order to obtain the highest temperature contrast without experimental artifacts

the best option to size a crack is using $d = -a$, i.e. when the laser spot is just touching the crack without overlapping it.

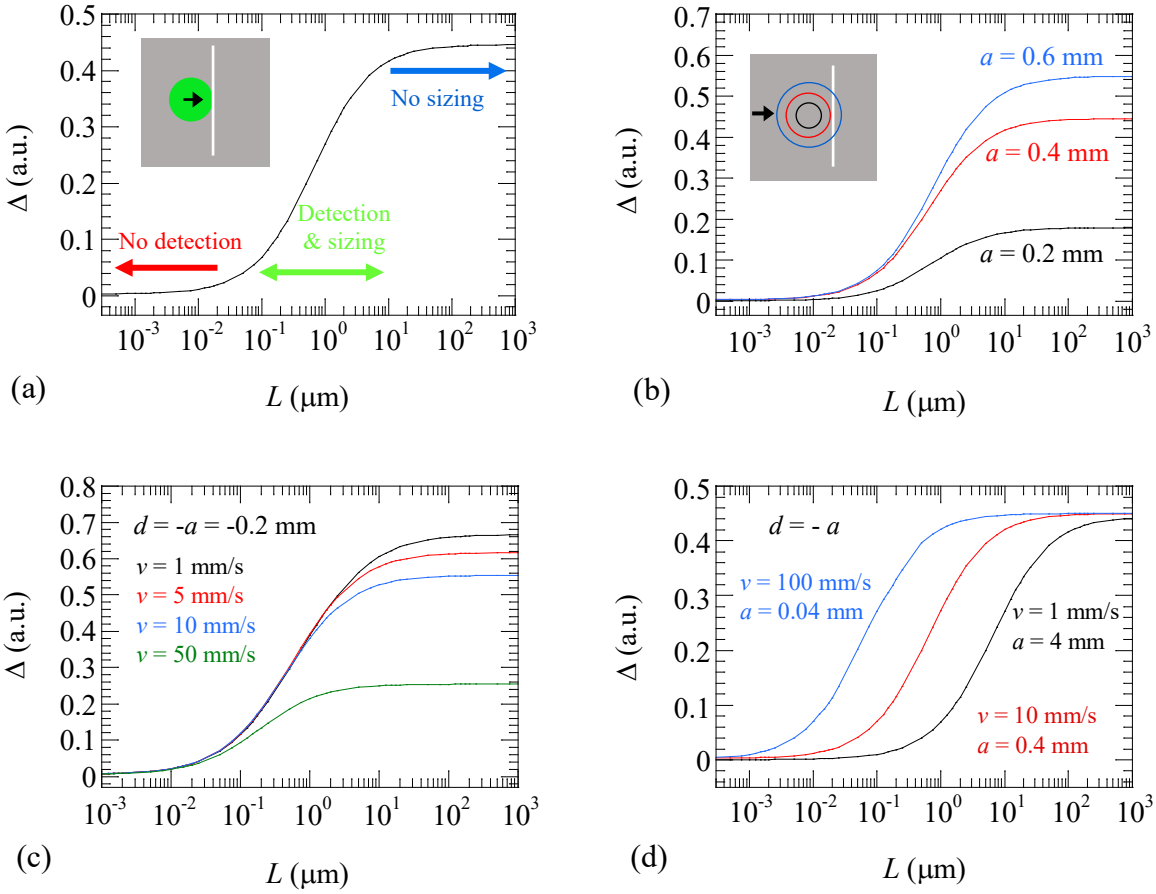

Figure 4. Simulations of temperature contrast as a function of the crack width in AISI-304. (a) $v = 10$ mm/s, $a = 0.4$ mm and $d = -a$. (b) Effect of the laser radius, $v = 10$ mm/s and $d = -0.4$ mm. (c) Effect of the laser speed, $a = 0.2$ mm and $d = -a$. (d) Effect of increasing the laser speed while decreasing the laser radius.

In Fig. 4c we evaluate the influence of the laser speed on the temperature contrast. Simulations are performed for AISI-304 with $d = -a = -0.2$ mm. Four speeds are considered. Simulations indicate that Δ decreases as the laser speed rises. This result alerts us about the difficulty of detecting cracks using a fast moving laser. However, this result is because we keep the laser radius constant as we increase the speed. In the simulations of Fig. 4d we reduce the laser radius by a factor of ten while increasing the laser speed by the same factor. Moreover, we keep the rule of $d = -a$. As can be observed, the highest temperature contrast remains unchanged, but the sigmoidal curve is shifted to the left by a factor of ten, i.e. the sensitivity is displaced to narrower cracks. It is worth mentioning that combining high speed and small radius

allows detecting and sizing cracks of submicronic width (see the blue line in Fig. 4d). Anyway, it is worth mentioning that the relationship $R_{th} = L/K_{air}$ is no longer valid when the width of the cracks is narrower than the mean free path of the air (≈ 0.1 μm at room temperature) [32]. Accordingly, for such a narrow cracks it is more accurate to give R_{th} than L.

According to the results of this section, we propose the following procedure to size cracks using Flying-Spot Thermography: (a) Using the temperature profile along the y-axis corresponding to the position of the laser spot just arriving to the crack ($d \approx -a$) and (b) selecting high speeds together with tightly focused laser spots for sizing extremely narrow cracks.

4. Experimental results and discussion

We have developed an IR thermography setup where the sample is moved at constant velocity while the laser spot remains at rest. The scheme of the setup is shown in Fig. 5. We use a CW-laser (532 nm, up to 6 W), which is directed to the sample surface perpendicularly using a small mirror glued to a Ge window, which reflects visible light and transmits IR wavelengths. The laser spot is focused by means of a 10 cm focal length lens to a radius at the sample surface in the range 300 - 400 μm. An IR video camera (FLIR, model SC7500, 320 × 256 pixels, pitch 30 μm and spectral band from 3 to 5 μm) records the temperature field at the sample surface at a frame rate between 1000 and 2000 images/s. The spatial resolution of the IR camera is improved up to 30 μm using an IR microscope lens. The corresponding field of view is 9.60 mm x 7.68 mm. The sample is mounted on a dynamic system (cart + track) that is coupled to an electric engine to move the cart at constant speed in the range between 1 and 100 mm/s.

To verify the ability of the Flying-Spot Thermography to size vertical cracks we have prepared AISI-304 stainless steel samples with calibrated vertical cracks. We put in contact two parallelepiped blocks of AISI-304. In order to calibrate the air gap between the two blocks we placed nickel tapes of equal thickness between them (10, 5 and 2.5 μm) and kept the blocks under pressure. In this way, the width of the air gap is equal to the thickness of the tapes. On the other hand, the surface of the blocks facing the IR camera is covered by a thin graphite layer (≈ 3 μm thick) to enhance both the absorption to the laser and the emissivity at infrared wavelengths.

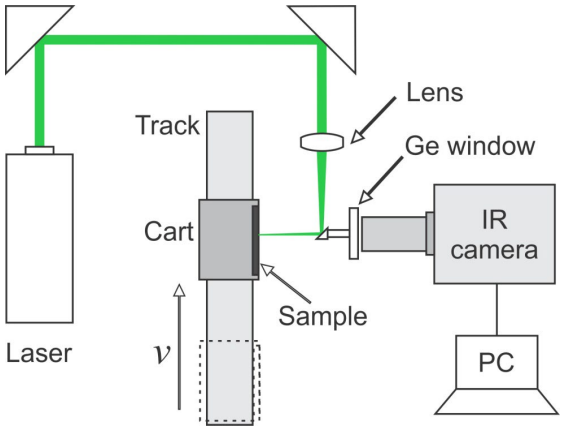

Figure 5. Scheme of the IR thermography setup with a moving sample and a resting laser spot.

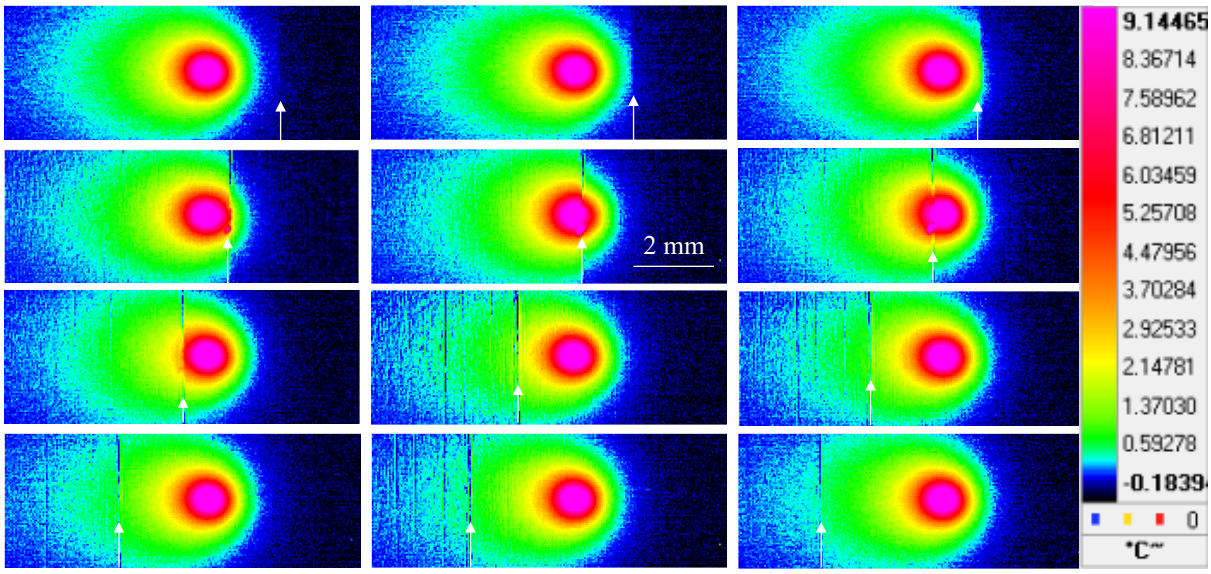

Figure 6. Sequence of thermograms corresponding to a crack with L = 0.56 μm in AISI-304. The laser is at rest while the sample is moving to the left at v = 3.56 mm/s. The laser power is P_o = 4 W and the radius is 0.4 mm. The arrow indicates the position of the crack.

We start measuring the case of two AISI-304 blocks put directly in contact without any nickel tape. Although the surfaces in contact are polished, the width of that crack is not zero due to the remaining slight roughness. In fact we measured the width using a lock-in thermography setup [5] and we found $L_{lock\text{-}in}$ = 0.56 μm. Figure 6 shows a sequence of thermograms corresponding to this sample. The white arrow indicates the position of the crack. Note that even for a so narrow fissure the temperature discontinuity is clearly marked. In order

to size the crack width we take the temperature profile along the horizontal line across the center of the laser spot and perpendicular to the crack.

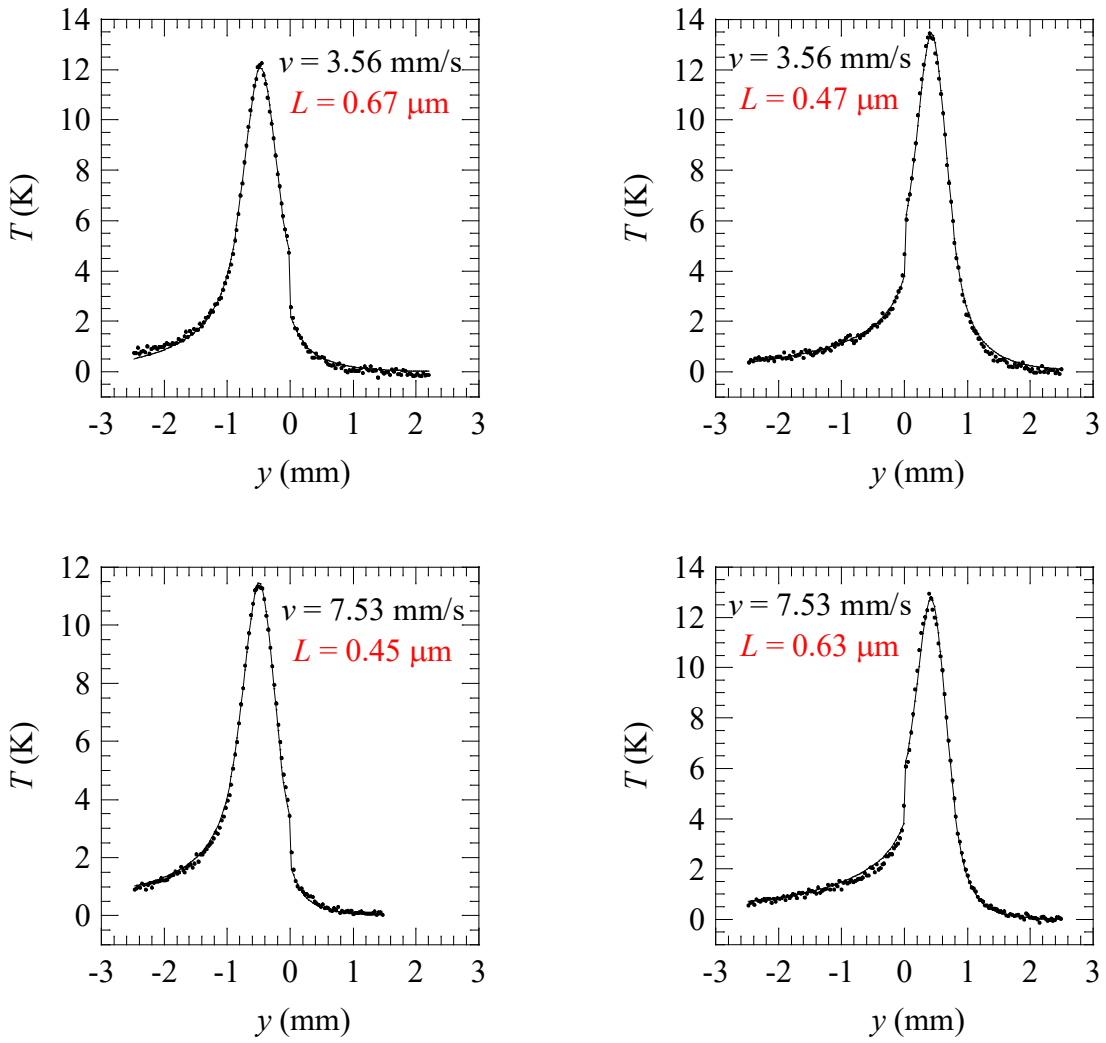

Figure 7. Temperature profiles corresponding to a crack 0.56 μm wide, for two positions of the crack, before and after reaching the laser, and for two sample speeds. Dots are the experimental data and the continuous lines the fit to Eq. (2). The retrieved crack width is indicated in red.

Figure 7 shows those profiles for two positions of the crack, before and after reaching the laser, and for two sample speeds. Dots are the experimental data and the continuous lines the fits to Eq. (2) using a nonlinear least square fitting function implemented on MATLAB. Temperature profiles described by Eq. (2) depend on 6 parameters: $P_o\eta/\varepsilon$, $KR_{th} = KL/K_{air}$, D, v, a, and t, which governs the distance between the laser spot and the crack. The thermal properties of the sample (D and K) and the thermal conductivity of air K_{air} = 0.025 $Wm^{-1}K^{-1}$ are taken

from the literature. Parameters v and t are measured very precisely from the IR video recorded by the camera due to the high acquisition frame rate. The radius of the laser spot a is measured optically. Accordingly, the only parameters involved in the fittings of the temperature profiles using Eq. (2) are: $P_o\eta/\varepsilon$ and L. The values in red in Fig. 7 correspond to the retrieved crack width. We have analyzed the profiles corresponding to all the thermograms verifying that the distance between the crack and the center of the laser spot is in the range 0.4-0.8 mm (i.e. between a and $2a$). The statistical analysis gives a crack width $L = 0.5\pm0.2$ µm, which is in good agreement with the lock-in thermography value indicating the reliability of the method. It is worth mentioning that the fitting of each profile is performed in less than one minute in a laptop.

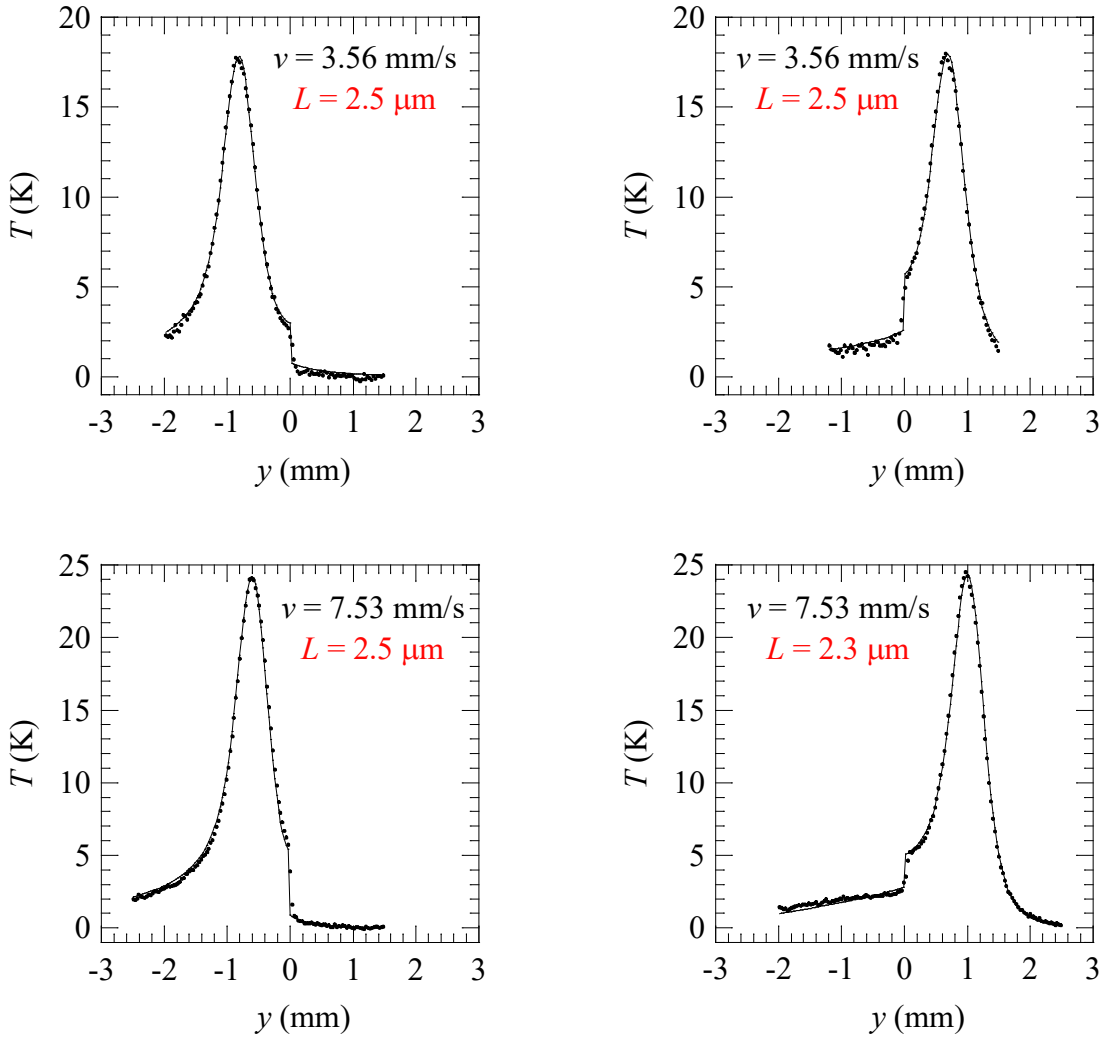

Figure 8. The same as in Fig. 7, but for a 2.5 µm wide crack. The retrieved crack width is indicated in red.

Similarly, Figs. 8 and 9 show two temperature profiles in the case of a nominal crack width of 2.5 μm (lock-in thermography measurements indicate $L_{lock\text{-}in}$ = 2.72 μm) and a nominal crack width of 10 μm ($L_{lock\text{-}in}$ = 10.5 μm), respectively. Dots are the experimental data and the continuous lines the fit to Eq. (2). The values in red correspond to the fitted widths. As before, we have analyzed the profiles corresponding to ~~all~~ the thermograms verifying that the distance between the crack and the center of the laser spot is in the range 0.4-0.8 mm. In the case of the 2.5 μm wide crack, the retrieved crack width is L = 2.5±0.4 μm, in very good agreement with the nominal value and showing a small uncertainty. However, for the 10 μm wide crack the retrieved width for v = 3.56 mm/s is L = 9.7±0.8 μm, whereas for v = 7.53 mm/s is L = 9±6 μm. This last result shows a huge uncertainty, even though the signal to noise ratio of the experimental data is excellent and the fits are very good. The reason for this uncertainty lies in the fact that for this combination of speed, radius and width, the temperature contrast is in the upper limit of the sizing region, very close to the boundary of the no sizing region, as it is shown by the red dot in Fig. 10. In this way, the mean value of the crack width is close to the real value, but the uncertainty is very high due to the sensitivity reduction. Unlike what happens for the thinner cracks studied in this work, the retrieved width value highly depends on the experimental parameters, in particular, the distance d between the center of the laser spot and the crack position.

It is worth noting that, provided the thermography setup works properly, the uncertainty in the retrieved crack widths mainly depends on the sensitivity given by the sigmoid Δ curve. When the Δ value falls in the middle of the sigmoid curve, as is the case of the green dots in Fig. 10, the uncertainty is around 20%. As the Δ value moves away from the maximum slope area, the uncertainty increases.

The results shown in this section confirm the ability of Constant Velocity Flying-Spot Thermography not only to detect narrow cracks, but also to size them. Anyway, it must be pointed out that for some combinations of speed, radius and width, fissures can be detected but not sized. In particular, for a given speed, the sigmoid of Δ is a guide to establish the upper value of the crack width that can be measured. It should be noted that Flying-Spot Thermography is not appropriate to size wide cracks, unless the laser (sample) speed is extremely low. Contrarily, this method is very efficient to size very narrow (submicronic) cracks, where other nondestructive techniques, as dye penetrant, fail. Anyway, it should be pointed out that high speed together with tightly focused laser beams requires IR cameras with high spatial resolution, approaching the diffraction limit of midwave IR cameras (3-5 μm).

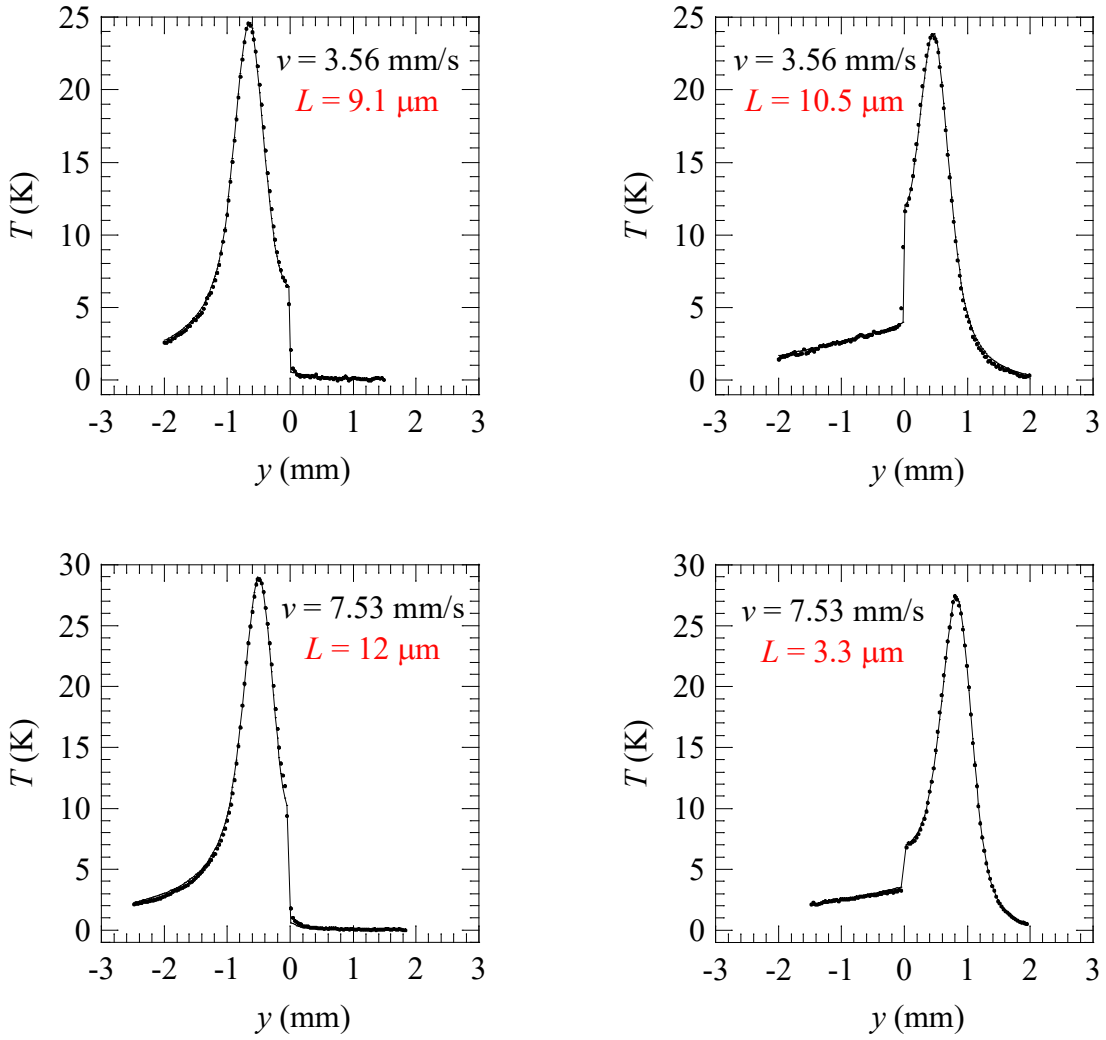

Figure 9. The same as in Fig. 7, but for a 10 μm wide crack. The retrieved crack width is written in red.

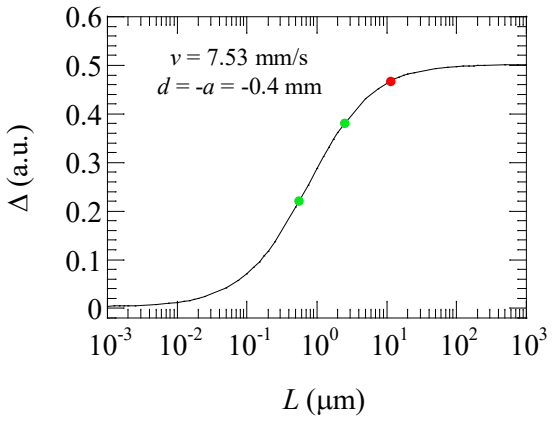

Figure 10. Simulations of temperature contrast as a function of the crack width in AISI-304 for v = 7.53 mm/s and d = -a = -0.4 mm. Dots indicate the value of Δ for the three crack widths studied in this work.

Before closing this section let us discuss the fact that there is a relationship between the maximum sample speed and the highest frame rate provided by the IR camera. Actually, in order to guarantee that there is at least one thermogram where the crack is close enough to the laser spot, the distance travelled by the crack between two consecutive thermograms (v/n, where n is the frame rate) must be smaller than the longitudinal thermal diffusion length ($\mu_y = D/v$ [30]). Accordingly, $v_{max} \leq \sqrt{nD}$. In this way, there is always a thermogram where the crack position is marked by a clear temperature jump.

5. Conclusion

Flying-Spot thermography has been used for more than two decades to detect cracks in opaque materials. In this work, we have proposed a method to size the width of infinite vertical cracks, for which an analytical expression of the surface temperature can be obtained. By fitting to this model the temperature profile along the axis that crosses the center of the laser spot and is perpendicular to the fissure, the width of the crack is obtained. Measurements performed in stainless steel samples with calibrated cracks in the range 0.5 – 10 μm confirm the validity of the method.

This method can be extended to more realistic cracks (finite vertical cracks, slanted cracks, cracks of irregular shape, etc.) in order to retrieve their geometry (length, depth, width, angle, etc.). However, for those realistic cracks, there is no analytical expression for the surface temperature and therefore the heat diffusion equation must be solved numerically. This will be the subject of future research. Anyway, let us to point out that the method proposed in this work could be applied for finite surface breaking vertical cracks provided that both length and depth are larger than twice the transverse thermal diffusion length, $\mu_{x,z} = 2D/v$ [30]. For instance, in stainless steel samples and v = 5 mm/s, cracks larger than 2 x 2 mm^2 behave as infinite.

Acknowledgments

This work has been supported by Ministerio de Economía y Competitividad (DPI2016-77719-R, AEI/FEDER, UE), by Gobierno Vasco (PIBA 2018-15), by Universidad del País Vasco UPV/EHU (GIU16/33) and by Conacyt (Beca Mixta 2017 Movilidad en el extranjero).

References

[1] X.P.V. Maldague, *Theory and Practice of Infrared Technology for Nondestructive Testing* (Wiley, New York, 2001).

[2] K.R. Grice, L.J. Inglehart, L.D. Favro, P.K. Kuo and R.L. Thomas, Thermal wave imaging of closed cracks in opaque solids, J. Appl. Phys. **54**, 6245-6255 (1983).

[3] A.M. Mansanares, T. Velinov, Z. Bozoki, D. Fournier and A.C. Boccara, Photothermal microscopy: thermal contrasta t grain interface in sintered metallic materials, J. Appl. Phys. 75, 3344-3350 (1994).

[4] F. Lepoutre, D. Balageas, Ph. Forge, S. Hirschi, J.L. Jouland, D. Rochais and F.C. Chen, Micron-scale thermal characterization of interfaces parallel or perpendicular to the surface, J. Appl. Phys. **78**, 2208-2223 (1995).

[5] N.W. Pech-May, A. Oleaga, A. Mendioroz, A.J. Omella, R. Celorrio and A. Salazar, Vertical cracks characterization using lock-in thermography: I. Infinite cracks, Meas. Sci. Technol., **25**, 115601 (2014).

[6] N.W. Pech-May, A. Oleaga, A. Mendioroz and A. Salazar, Fast characterization of the width of vertical cracks using pulsed laser spot infrared thermography, J. Nondestruct. Eval. **35**, 22 (2016).

[7] M. Streza, Y. Fedala, J.P. Roger, G. Tessier and C. Boue, Heat transfer modelling for surface crack depth evaluation, Meas. Sci. Technol. **24**, 045602 (2013).

[8] Y. Fedala, M. Streza, J.P. Roger, G. Tessier and C. Boue, Open crack depth sizing by laser stimulated infrared lock-in thermography, J. Phys. D: Appl. Phys. **47**, 465501 (2014).

[9] R. Celorrio, A.J. Omella, N.W. Pech-May, A. Oleaga, A. Mendioroz and A. Salazar, Vertical cracks characterization using lock-in thermography: II. Finite cracks, Meas. Sci. Technol., **25**, 115602 (2014).

[10] E.J. Kubiak, Infrared detection of fatigue cracks and other near-surface defects, Appl. Opt. **7**, 1743-1747 (1968).

[11] H.E. Cline and T.R. Anthony, Heat treating and melting material with scanning laser or electron beam, J. Appl. Phys. **48**, 3895 (1977).

[12] Y.Q. Wang, P.K. Kuo, L.D. Favro and R.L. Thomas, A novel "flying-spot" infrared camera for imaging very fast thermal-wave phenomena, In Photoacoustic and Photothermal Phenomena II Springer Series in Optical Sciences **62**, 24-26 (1990).

[13] J.L. Bodnar, M. Egée, C. Menu, R. Besnard, A. Le Blanc, M. Pigeon and J.Y. Sellier, Cracks detection by a moving photothermal probe, J. de Physique IV, Colloque C7 **4**, C7-591-594 (1994).

[14] J.L. Bodnar and M. Egée, Wear crack characterization by photothermal radiometry, Wear **196**, 54-59 (1996).

[15] C. Gruss and D. Balageas, Theoretical and experimental applications of the flying spot camera, QIRT Conference Paris 1992. Available from QIRT Open Archives: http://dx.doi.org/10.21611/qirt.1992.004.

[16] J.C. Krapez, Résolution spatiale de la camera thermique à source volante, Int. J. Therm. Sci. **38**, 769-779 (1999).

[17] T. Li, D.P. Almond and D.A.S. Rees, Crack imaging by scanning laser-line thermography and laser-spot thermography, Meas. Sci. Technol. **22**, 035701 (2011).

[18] J. Schlichting, M. Ziegler, A. Dey, Ch. Maierhofer and M. Kreutzbruck, Efficient data evaluation for thermographic crack detection, QIRT J. **8**, 119-123 (2011).

[19] T. Li, D.P. Almond and D.A.S. Rees, Crack imaging by scanning pulsed laser spot thermography, NDT&E Int. **44**, 216-225 (2011).

[20] S.E. Burrows, S. Dixon, S.G. Pickering, T. Li and D.P. Almond, Thermographic detection of surface breaking defects using scanning laser source, NDT&E Int. **44**, 589-596 (2011).

[21] J. Schlichting, Ch. Maierhofer and M. Kreutzbruck, Defect sizing by local excitation thermography, QIRT J. **8**, 51-63 (2011).

[22] J. Schlichting, Ch. Maierhofer and M. Kreutzbruck, Crack sizing by laser excited thermography, NDT&E Int. **45**, 133-140 (2012).

[23] T. Maffren, P. Juncar, F. Lepoutre and G. Deban, Crack detection in high-pressure rurbine blades with flying spot active thermography in the SWIR range, Rev. Progress Quantitative Nondestructive Evaluation, AIP Conference Proc. **1430**, 515-522 (2012).

[24] U. Netzelmann, Flying-spot lock-in thermography and its application to thickness measurement and crack detection, QIRT Conference Bordeaux 2014. Available from QIRT Open Archives: http://dx.doi.org/10.21611/qirt.2014.064.

[25] A. Thiam, J.C. Kneip, E. Cicala, Y. Caulier, J.M. Jouvard and S. Mattei, Modeling and optimization of open crack detection by flying spot thermography, NDT&E Int. **89**, 67-73 (2017).

[16] N. Montinaro, D. Cerniglia and G. Pitarresi, Detection and characterization of disbonds on fibre metal laminate hybrid composites by flying laser spot thermography, Composites Part B **108**, 164-173 (2017).
[27] C. Boué and S. Holé, Open crack depth sizing by multi-speed continuous laser stimulated lock-in thermography, Meas. Sci. Technol. **28**, 065901 (2017).
[28] L. Gaverina, A. Sommier, J.L. Battaglia, J.C. Batsale and C. Pradere, Pulsed flying spot with the logarithmic parabolas method for the estimation of in-plane thermal diffusivity fields on heterogeneous and anisotropic materials, J. Appl. Phys. **121**, 115105 (2017).
[29] L. Gaverina, A. Sommier, J.L. Battaglia, J.C. Batsale and C. Pradere, Pulsed flying spot elliptic method for the estimation of the thermal diffusivity field of orthotropic materials, Int. J. Therm. Sci. **125**, 142-148 (2018).
[30] A. Bedoya, J. González, J. Rodríguez-Aseguinolaza, A. Mendioroz, A. Sommier, J.C. Batsale, C. Pradere and A. Salazar, Measurement of in-plane thermal diffusivity of solids moving at constant velocity using laser spot infrared thermography, Measurement **134**, 519-526 (2019).
[31] Carslaw H S and Jaeger J C 1959 *Conduction of Heat in Solids* (Oxford: Oxford University Press) p. 20.
[32] M. Beyfuss, J. Baumann and R. Tilgner, Photothermal imaging of local thermal resistances, in Photoacoustic and Photothermal Phenomena II. Murphy J.C., Spicer J.W.M., Aamodt L.C., Royce B.S.H. (eds), Springer Series in Optical Sciences **62**, 17 (1990).